Research Paper

Theoretical and Numerical Analyses of an Aluminium-Concrete Composite Beam with Channel Shear Connectors

Łukasz POLUS*, Maciej SZUMIGAŁA

Faculty of Civil and Environmental Engineering
Poznan University of Technology
Piotrowo 5, 60-965 Poznan, Poland
*Corresponding Author e-mail: lukasz.polus@put.poznan.pl

This paper presents a numerical simulation and a theoretical investigation of an aluminium-concrete composite (ACC) beam subjected to bending. ACC structures are similar to steel-concrete composite (SCC) structures. However, their girders are made of aluminium instead of steel. The use of ACC structures is limited because of the lack of relevant design rules. Due to this fact the authors suggest applying the theory for SCC structures to ACC structures. In this paper, the methods for calculating the bending resistance and the stiffness of ACC beams were presented. What is more, the results from the theoretical investigation were compared with the results from the laboratory tests conducted by Stonehewer in 1962. The calculated plastic resistance moment of the ACC beam with partial shear connection was 1.2 times lower than the bending resistance from the laboratory test. The calculated stiffness was 1.1 higher than the stiffness from the laboratory test. What is more, the authors of this paper prepared two numerical models of the ACC beam. The analysed models had different types of connection between the aluminium beam and the concrete slab. In the first variant, the aluminium beam was permanently connected with the concrete slab to model full composite action. In the second variant, the aluminium beam and the concrete slab were connected using zero-length wires, the characteristics of which were taken from the laboratory test, to take slip into account. The numerical model with zero-length springs adequately captured the elastic response of the ACC beam from the laboratory test conducted by Stonehewer.

Key words: aluminium-concrete composite beam; slip; aluminium; concrete damaged plasticity model; channel shear connector; finite element method.

1. Introduction

Connections play a crucial role in composite elements. They decide about the behaviour of a composite beam. Shear connectors are still being developed and new solutions, such as like puzzle-shaped composite dowels, are more often used [1, 2]. Sometimes the number of shear connectors is insufficient to ensure full composite action and a beam behaves like a partial composite beam in some

slip in the connection [3]. This problem often appears in composite structures, especially when a concrete slab has profiled sheeting and the number of shear connectors is insufficient to prevent slipping because the number of the ribs in the profiled sheeting is limited [4]. The role of the shear connection between the steel element and the concrete slab is well understood in composite beams with full interaction [5]. However, it calls for more investigation in beams with incomplete interaction. The shear connection may be rigid or flexible [5]. In composite beams with rigid connection, slipping in the connection interfaces is small and the impact of the slipping on the stiffness and the load bearing capacity is negligible. In composite beams with flexible connection, the impact of the slipping in the connection on the stiffness and the load bearing capacity is significant. The effects of partial interaction may be taken into account by using the effective value of the bending stiffness.

Kuczma M. and Kuczma B. analysed steel-concrete composite beams with stud shear connectors or an adhesive, and they prepared a mathematical model of a SCC beam with partial interaction and slipping in the place of connection between both materials [6]. The problem of slipping does not only appear in SCC structures. It also affects the load bearing capacity and the stiffness of composite elements made of different materials, e.g., timber-composite structures [7]. Numerical models of the composite beams should take slip into account when it is significant – for beams with incomplete interaction. For instance, the slip was taken into account in the numerical model of the connection for timber-concrete composite beams with profiled sheeting [8] by modelling the connection using zero-length wires. The characteristics of these wires were taken from the laboratory push-out test. The same solution was used for an aluminium-concrete composite beam with profiled sheeting [9]. However, the problem with the slipping in connection may also appear in composite beams with solid concrete slabs. In this paper, the authors analysed an aluminium-concrete composite beam with aluminium channel shear connectors, subjected to bending. In the analysed beam the slip occurred despite the fact that it did not have profiled sheeting. Taking into account the problems mentioned above, the main goals of this paper are:

- suggesting the methods for calculating the bending resistance and the stiffness of ACC beams,
- developing a numerical model of the ACC beam with aluminium channel shear connectors, in which the slip will be taken into account.

1.1. Advantages and disadvantages of aluminium-concrete composite (ACC) structures

The combination of aluminium and concrete is not a new idea. Both aluminium-concrete columns and aluminium-concrete beams were tested in the past. Concrete-

filled aluminium columns have high strength thanks to aluminium and high stiffness thanks to concrete [10–12]. Aluminium-concrete beams combine the advantages of these two materials [13, 14]. They have been successfully used in a number of bridges [15–18]. ACC structures have advantages which, in some situations, make them the best choice. However, they also have disadvantages, which should be analysed before ACC structures are used.

Thanks to corrosion resistance, aluminium elements do not need to be painted [19, 20]. However, aluminium parts which are in contact with wet concrete are exposed to corrosion due to alkali. For this reason, such aluminium elements should be painted. Stonehewer recommended securing aluminium with a paint system consisting of one coat of wash primer, one coat of zinc chromate primer, and one coat of alkali-resistant bituminous paint [21]. Aluminium may also corrode when it is in contact with steel (galvanic corrosion). This contact may take place between the aluminium elements embedded in a concrete slab and the reinforcing steel bars, the aluminium beam and the steel shear connectors, or between the aluminium beam and the profiled steel sheeting. For this reason, aluminium should be insulated, e.g., connectors may be galvanised. Unfortunately, connectors may lose plating as a result of friction. High-strength stainless steel friction grip bolts may solve this problem. However, they are expensive.

Due to its light weight, an aluminium structure may be erected from prefabricated portions, which are easy to transport [22]. During the cutting of aluminium elements sparks are not produced [23]. Moreover, aluminium beams may have optimal cross-sections and are easily produce through extrusion [24]. Thin-walled aluminium elements may be produced using the roll-forming method, which is more cost-effective than extrusion [25].

An aluminium beam works efficiently with a concrete slab, due to the relative closeness of the Young's moduli of the two materials [26]. Due to its lower modulus, aluminium is more resistant to impulse loads than steel [27]. However, owing to fact that the modulus of elasticity of aluminium is three times lower than that of steel, significant deflections may occur [28].

Aluminium-concrete composite elements may be used outdoors, because of the excellent low-temperature toughness of aluminium alloys. They are exposed to static and dynamic loads. It is crucial to study the behaviour of materials under low and high strain rate loading. For example, the strain rate sensitivity of the AW-6060 T6 aluminium alloy is close to none at room temperature [29].

The use of aluminium-concrete structures may be limited due to the high initial cost of aluminium. However, aluminium does not need periodic painting, which may result in a lower total cost over the entire life of a structure. The next problem is the lack of design rules for aluminium-concrete composite structures. Designers will not risk the using ACC structures without having appropriate standards. Aluminium also has a lower fatigue strength than steel [30]. More-

over, thermal stresses and different values of thermal expansion may appear in aluminium-concrete composite elements, because aluminium and concrete have different thermal expansion coefficients [31]. In older solutions, anchorages were used to solve the problem of different values of thermal expansion of the aluminium elements and the concrete slab. What is more, it is difficult to repair aluminium structural elements after an accident, because welding or straightening with the use of heat creates heat-affected zones and causes the reduction of strength parameters [32, 33]. Furthermore, the fire resistance of aluminium elements is very low, because of the rapid reduction of the yield strength in high temperatures [34–36].

1.2. *Shear connectors for aluminium-concrete composite (ACC) structures*

To join an aluminium beam with a concrete slab one may use shear connectors made of: Z-type elements [37], channels [21], angles [37], bolts [13] or dowel-bolt connectors presented in [38].

1.3. *The aluminium-concrete composite (ACC) beam tested by* STONEHEWER *[21]*

Stonehewer conducted four groups of tests: bond tests of aluminium rods embedded in concrete, push-out tests of aluminium shear channel connectors, static bending tests of aluminium-concrete composite beams and tests of materials parameters. He tested two ACC beams with different spans. The dimensions and the material parameters of the shorter beam were used in this article to prepare a numerical model of the ACC beam in the Abaqus software and to conduct the theoretical investigation. The shorter beam was a partial composite beam consisting of an aluminium beam, a concrete slab, a reinforcing mesh and twelve shear channel connectors. The yield strength and the Young's modulus of the magnesium-silicon aluminium alloy were 275.79 MPa and 65.98 GPa respectively. The concrete cylinder strength was 26.89 MPa and the modulus of elasticity of the concrete was 22.41 GPa. The reinforcing mesh was made of a welded cold drawn wire with a diameter of 4.1 mm. The square opening size of the mesh was 101.6×101.6 mm.

2. PROBLEM FORMULATION

Designers use standards when preparing their projects. Because of the lack of design rules for ACC structures they do not use these elements. Due to this fact, the authors of this paper as well as STONEHEWER [21], BRUZZESE *et al.* [13] suggest applying the theory for SCC structures to ACC structures. Research papers [13, 21] are quite out-of-date, and for this reason the present authors

proposed the methods for calculating the bending resistance and the stiffness of ACC beams based on the theory for SCC structures available in the most recent standards and articles. The above mentioned methods were used to evaluate the bending resistance and the stiffness of the ACC beam with channel shear connectors tested by Stonehewer in 1962 (see Fig. 1). To evaluate how effective and safe these methods are, the results from the theoretical investigation were compared with the results from the laboratory tests conducted by Stonehewer. What is more, the present authors decided to evaluate the reduction of the stiffness and the bending resistance of the ACC beam caused by the slip. They prepared two numerical models of the ACC beam with different connections between the aluminium beam and the concrete slab. In the first model, the aluminium beam was permanently connected with the concrete using the *tie* function to create a full composite beam. In the second model, the aluminium beam was connected with the concrete slab using zero-length wires. The wires behaved like non-linear springs to allow slipping between the aluminium beam and the concrete slab. The characteristics of a single spring reflected the load-end slip curve of a single channel connector from the bending test conducted by Stonehewer (see Fig. 2). The present authors could also have taken into
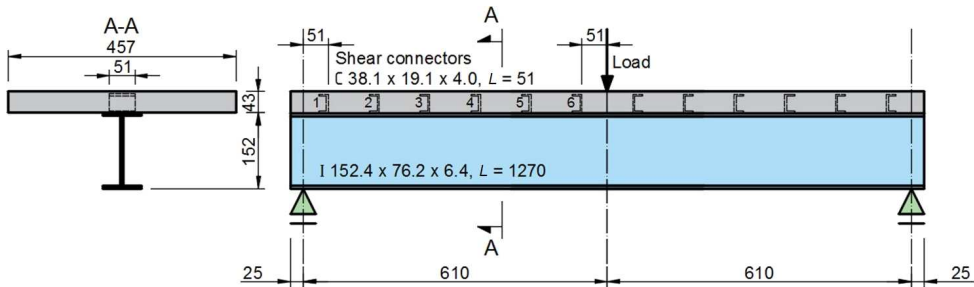

FIG. 1. The aluminium-concrete composite beam tested by STONEHEWER [21].
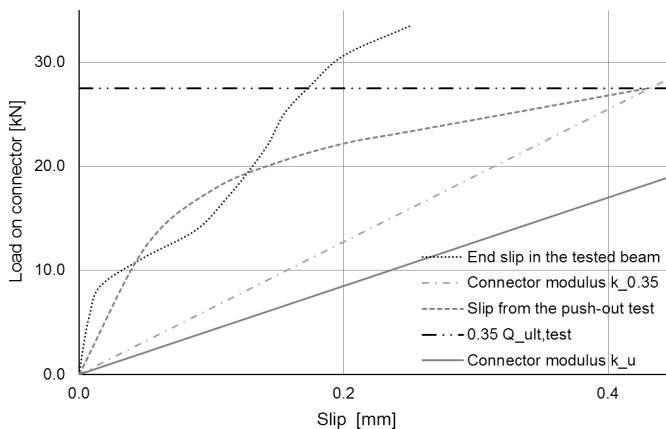

FIG. 2. Load-slip curves from the laboratory bending and push-out tests [21].

account the load-slip curve from the push-out test of the connectors instead
of the load-end slip curve from the bending test. The results of the theoretical and
the numerical analyses were compared with the results from Stonehewer's tests.
Stonehewer tested the partial composite beam. The present authors expected
that the results from the theoretical analysis of the partial ACC beam and the
results from the numerical model which took slip into account would correspond
to the results from Stonehewer's test.

3. Theoretical background

In this section, the authors presented the methods for calculating: elastic re-
sistance to bending of an ACC beam, plastic resistance to bending of a full com-
posite aluminium-concrete beam, plastic resistance to bending of an aluminium-
concrete beam with partial shear connection, bending stiffness of a full compos-
ite aluminium-concrete beam, and effective value of the bending stiffness of an
aluminium-concrete beam with partial shear connection, based on the theory
for SCC structures [39–42]. The above mentioned methods are presented in the
theoretical analyses of the ACC beam tested by STONEHEWER in 1962 [21].

The elastic resistance to bending of the ACC beam was calculated with the
following assumptions: normal stress in aluminium beam flanges did not exceed
the yield strength of aluminium and normal stress in concrete did not exceed
the compressive strength of concrete. The cross-section of the ACC beam was
replaced with an ideal cross-section with reduced slab width using modular ra-
tio n (the ratio between the modulus of elasticity of aluminium and the modulus
of elasticity of concrete). To take into account the long term effects of creep
and shrinkage, the modulus of elasticity of concrete in the theoretical analysis
was twice lower than the modulus of elasticity of concrete from the laboratory
test conducted by Stonohewer. The ideal cross-section of the analysed composite
beam is presented in Fig. 3. The calculation of the elastic resistance to bending
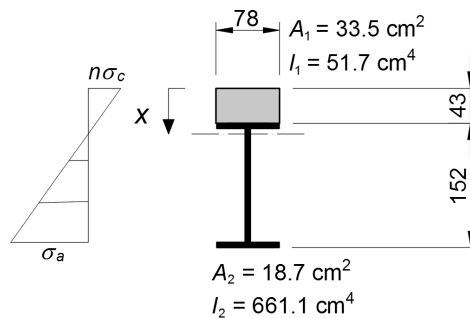of the ACC beam is presented in Table 1.

FIG. 3. Ideal cross-section of the ACC beam.

Table 1. The calculation of the elastic resistance to bending of the ACC beam.

Parameter	Value
Modular ratio n [–]	5.89
Area of the ideal cross-section A [cm^2]	52.2
First moment of area of the aluminium beam (for the top fibre of the slab) S_a [cm^3]	72.0
First moment of area of the slab (for the top fibre of the slab) [cm^3] S_c	222.5
Position of centroid axis x [cm]	5.6
Second moment of area of the ideal cross-section I_y [cm^4]	1853.7
Section modulus of the ideal cross-section W_y [cm^3]	133.4
Elastic resistance to bending of the cross-section of the ACC beam M_{el} [kN·m]	36.8

In the elastic range, shear connectors should be able to resist the longitudinal shear flow. It was calculated according to the elastic theory and using the formula presented in [41] (Żurawski's equation):

$$(3.1) \qquad V_L = \frac{V A_e z}{I_y},$$

where V – shear force at the cross-section, A_e – effective area above the neutral axis, and the level considered in the ideal cross-section, z – vertical distance between the neutral axis of the ideal cross-section and the centroid of the effective area, I_y – second moment of area of the ideal cross-section.

The calculation of the shear flow for one force in the mid-span is presented in Table 2.

Table 2. The calculation of the shear flow of the ACC beam.

Parameter	Value
Shear force V [kN]	60.3
Effective area A_e [cm^2]	33.5
Vertical distance from the neutral axis to the centroid of effective area z [cm]	3.5
Longitudinal shear flow V_L [kN/cm]	3.8

The diagram of the elastic shear flow was rectangular in a three-point bending test. The shear flow was 3.8 kN/cm. The longitudinal force was equal to the area under the diagram of the elastic shear flow: 3.8 kN/cm · 61.0 cm = 231.8 kN. The spacing of the channel shear connectors was 101.6 mm. There were 6 connectors placed within the critical length. The total resistance of the 6 connectors (6 · 71.26 = 427.6 kN) was greater than the longitudinal force and it was possible to achieve elastic bending resistance of the ACC beam. The nom-

inal shear strength of the channel shear connector (71.26 kN) was determined from [43] as:

$$(3.2) \qquad Q_{ult} = 0.3(t_f + 0.5t_w)l_a\sqrt{f_c'E_c},$$

where l_a – length of the channel shear connector [mm], t_f – thickness of the channel shear connector flange [mm], t_w – thickness of the channel shear connector web [mm], E_c – modulus of elasticity of concrete [MPa], f_c' – compressive strength of concrete [MPa].

In 1962 Stonehewer used the resistance of the connector as the useful channel shear connector capacity [21]. It was determined from:

$$(3.3) \qquad Q_y = (t_f + 0.5t_w)l_a\sqrt{f_c'f_y},$$

where Q_y – useful capacity of the connector [kips], l_a – length of the channel shear connector [inches], t_f – thickness of the channel shear connector flange [inches], t_w – thickness of the channel shear connector web [inches], f_c' – compressive strength of concrete [kips per square inch], f_y – yield strength of connector material [kips per square inch].

In his opinion, formula (3.3) may determine the moment when the channel connector starts to yield and when slipping occurs.

The plastic resistance to bending of the cross-section of the ACC beam was calculated using the assumption that normal force in the aluminium beam section was equal to the normal force in the concrete slab. In the analysed example, the aluminium girder had a class 3 cross-section, for which plastic bending resistance should not be calculated and used during designing. However, the authors of this paper calculated the plastic bending resistance to present a complete theoretical analysis. The neutral axis was in the top flange of the aluminium beam.

Table 3. The calculation of the plastic resistance to bending of the cross-section of the ACC beam.

Parameter	Value
Normal force in the aluminium beam T [kN]	515.7
Position of neutral axis x_{pl} [cm]	4.9
Plastic resistance to bending M_{pl} [kN·m]	47.1
Normal force in the concrete slab F [kN]	449.2

The degree of the shear connection was $\eta = 6 \cdot 71.26/449.2 = 0.95$. Because it was lower than 1.0, the analysed element was a partial composite beam. The

plastic resistance to bending of the ACC beam with the partial shear connection tested by Stonehewer was calculated using the following formula [39]:

$$(3.4) \qquad M_{pl,\eta} = M_{pl,a} + (M_{pl} - M_{pl,a})\eta,$$

where $M_{pl,a}$ – plastic resistance of the aluminium section.

Table 4. The calculation of the plastic resistance to bending of the cross-section of the aluminium-concrete composite (ACC) beam with partial shear connection.

Parameter	Value
Plastic resistance of the aluminium section $M_{pl,a}$ [kN·m]	24.0
Plastic resistance to bending of the ACC beam with partial shear connection $M_{pl,\eta}$ [kN·m]	45.9

The stiffness of the full composite aluminium-concrete beam corresponds to the stiffness of the transformed section of the composite beam $(EI)_e$.

The effective stiffness of the partial composite ACC beam may be calculated based on the calculation model for a steel-concrete composite beam presented in the articles [3, 4]. It was assumed that the shear stress at the interface was proportional to the slip and that the aluminium girder and the concrete slab had the same curvature. The calculation was prepared for the case of the simply supported beam with a single load.

The effective stiffness of the partial composite ACC beam was calculated as [3, 4]:

$$(3.5) \qquad (EI)_{eff} = \frac{(EI)_e}{(1 + \xi_s)},$$

where $(EI)_e$ – stiffness of the transformed section of the composite beam, ξ_s – parameter for the slip effect.

The parameter for the slip effect was calculated as [3, 4]:

$$(3.6) \qquad \xi_s = \eta \left[0.5 - \frac{1}{\alpha L} \right],$$

where $\eta = 24(EI)_e \beta/(L^2 h)$, L – span length, h – depth of the entire section,

$$\alpha = \sqrt{\frac{K}{E_s I_0 A_1 p}}, \qquad \beta = \frac{A_1 d_c p}{K}, \qquad d_c = h_c/2 + y_1,$$

h_c – thickness of the concrete slab, y_1 – distance from the top of the aluminium girder to its neutral axis, p – longitudinal spacing of shear connectors,

$$A_1 = \frac{A_0}{d_c^2 A_0 + I_0}, \qquad A_0 = \frac{A_a A_c}{n A_a + A_c}, \qquad I_0 = I_a + I_c/n,$$

n – modular ratio, A_a – area of aluminium section, A_c – area of concrete section, I_a – moment of inertia of aluminium, I_c – moment of inertia of concrete, K – shear stiffness of the connector.

The authors of this paper calculated the shear stiffness of the connector based on the load-slip curve from the push-out test presented in [21] (see Fig. 2). In timber-concrete composite structures and steel-timber composite structures two different slip moduli are considered for design purposes: k_{ser} for the serviceability limit state and k_u for the ultimate limit state [44–46]. The slip modulus k_{ser} corresponds to the secant value at 40% of the load-carrying capacity ($k_{0.4}$). The slip modulus k_u corresponds to the secant value at 60% of the load-carrying capacity ($k_{0.6}$). Because Stonehewer did not publish all of his results, the authors of this paper used $k_{0.35}$ instead of $k_{0.4}$. What is more, they calculated $k_u = 2/3k_{0.35}$ as recommended in [47] and used the modulus k_u as the shear stiffness of the connector K.

The results from this paragraph are summarised in the Results section.

Table 5. The calculation of the effective stiffness of the aluminium-concrete composite (ACC) beam with partial shear connection.

Parameter	Value
Span length L [cm]	122
Depth of the entire section h [cm]	19.5
Thickness of the concrete slab h_c [cm]	4.3
Moment of inertia of aluminium I_a [cm^4]	661.1
Moment of inertia of concrete I_c [cm^4]	302.9
Modular ratio n [–]	5.89
Moment of inertia I_0 [cm^4]	712.5
Area of aluminium section A_a [cm^2]	18.7
Area of concrete section A_c [cm^2]	196.5
Distance from the top of the aluminium girder to its neutral axis y_1 [cm]	7.6
Dimension d_c [cm]	9.8
Shear stiffness of the connector K [kN·cm]	425
A_0 [cm^2]	12.0
A_1 [cm^2]	0.006
Longitudinal spacing of shear connectors p [cm]	10.2
Coefficient α [–]	0.037
Coefficient β [–]	0.0015
Coefficient η [–]	1.53
Parameter for the slip effect ξ_s [–]	0.43
Stiffness of the transformed section of the composite beam $(EI)_e$ [kN·cm^2]	12 230 713
The effective stiffness $(EI)_{eff}$ [kN·cm^2]	8 577 514

4. The numerical models

Two numerical models were prepared in the Abaqus software. They differed only in the type of connection between the aluminium part and the concrete element. One model consisted of a concrete slab, an aluminium beam, shear channel connectors, a steel plate and a reinforcing mesh (see Figs 4a and 4b).
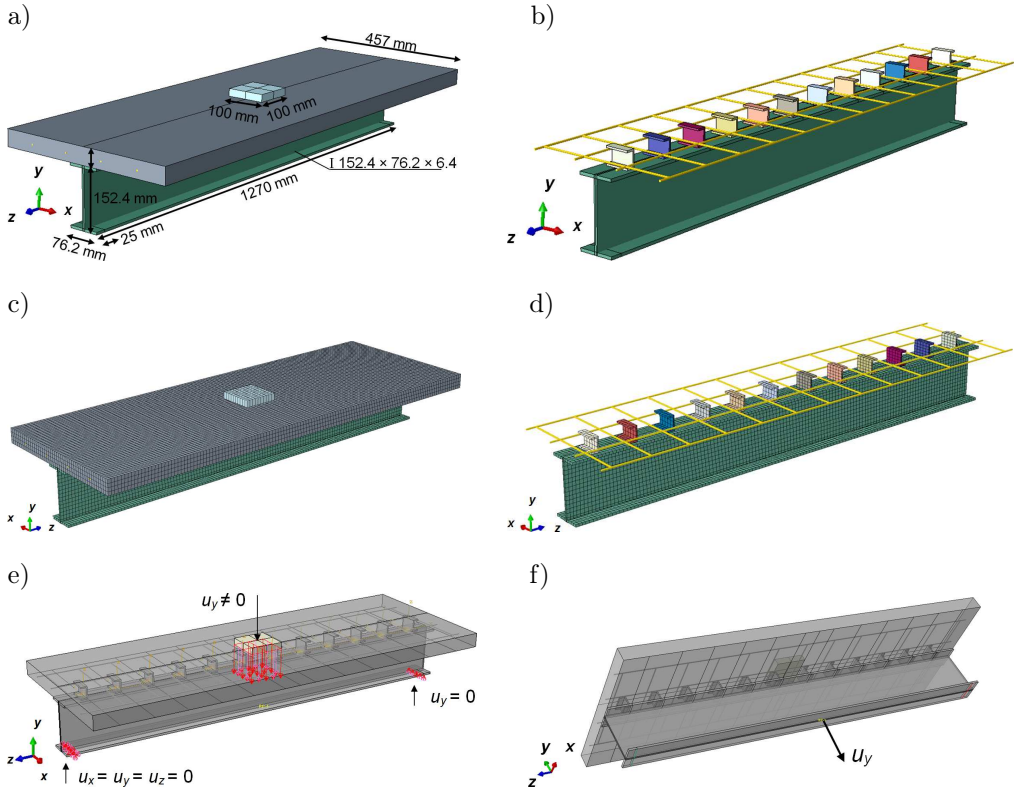

Fig. 4. Numerical model of the ACC beam: a) complete model; b) aluminium beam with the reinforcing mesh and the shear channel connectors; c) ACC beam mesh; d) aluminium beam mesh; e) boundary condition; f) location of the deflection measured point.

The concrete slab and the channel connectors were divided into eight-node cuboidal finite solid elements (C3D8R), the reinforcing mesh was modelled by means of truss elements (T3D2), the steel plate and the aluminium beam was divided into four-node shell elements (S4R). The mesh size was 14 mm. The total number of all elements was 11 783 (see Figs 4c and 4d). The reinforcing mesh and the shear channel connectors were embedded in the concrete slab. The calculations were performed using the Newton-Raphson method in the Abaqus software. The steel sheet was joined with the concrete slab and was used to apply the vertical displacement ($u_y \neq 0$) (see Fig. 4e). The ACC beam was supported

linearly in two places. In the first support, displacements in x, y, and z directions were fixed. In the second support, displacement in y direction was fixed. The midspan deflection was measured in the reference point on the aluminium beam (see Fig. 4f). The aluminium was modelled as a linear elastic-plastic material with strain hardening (Young's modulus = 65.98 GPa, yield strength = 275.79 MPa, ultimate strength = 303.37 MPa, Poisson's ratio = 0.3). The engineering values of stress and strain were transformed into the true values of stress and strain. The true stress and the logarithmic true strain were used in the Abaqus system [48]. The behaviour of concrete was captured using the *concrete damaged plasticity* (CDP) model described in [49, 50] and successfully used, e.g., by SZEWCZYK and SZUMIGAŁA [51]. The parameters used in the model are summarised in Tables 6–8.

Table 6. Parameters of concrete used in numerical calculations.

Parameter	Value
Young's modulus E_{cm} [MPa]	22 410
Poisson's ratio ν [–]	0.20
Mean value of concrete cylinder compressive strength f_{cm} [MPa]	26.89
Mean value of axial tensile strength of concrete f_{ctm} [MPa]	2.2
Largest nominal maximum aggregate size d_a [mm]	8.0
Fracture energy G_F [N/m]	51.0
Parameter n [–]	0.7
Dilatation angle [°]	40.0
Eccentricity [–]	0.1
f_{b0}/f_{c0} [–]	1.16
Parameter κ [–]	0.667
Viscosity parameter [–]	0.01

The stress-strain diagram for the analysis of the concrete subjected to compression or tension was adopted from [52] or [53]. The compressive strength of the concrete was based on Stonehewer's laboratory tests [21], and the tensile strength of the concrete was taken from [52] for the C20/25 concrete. The value of the critical crack opening and the fracture energy were calculated using the formulas presented in [53–56]. The parameters used in the CDP model were calculated in accordance with the formulas presented in article [57]. The analysed models had different connection types between the aluminium beam and the concrete slab. The shear channel connectors were used in the model to increase its stiffness, but not to join the aluminium beam and the concrete slab in the numerical model, because this connection was modelled in an indi-

Table 7. Material parameters used in the *concrete damaged plasticity* (CDP) model of concrete subjected to compression.

Concrete compression hardening		Concrete compression damage	
Stress [MPa]	Crushing strain [–]	D_c [–]	Crushing strain [–]
6.71	0.00000000	0.000	0.00000000
17.73	0.00010905	0.000	0.00010905
20.58	0.00018178	0.000	0.00018178
22.96	0.00027558	0.000	0.00027558
25.20	0.00042542	0.000	0.00042542
26.69	0.00065887	0.000	0.00065887
26.89	0.00080009	0.000	0.00080009
26.87	0.00085110	0.001	0.00085110
26.68	0.00095932	0.008	0.00095932
26.52	0.00101664	0.014	0.00101664
26.04	0.00113797	0.032	0.00113797
25.35	0.00126864	0.057	0.00126864
24.45	0.00140915	0.091	0.00140915
23.31	0.00156004	0.133	0.00156004
20.27	0.00189537	0.246	0.00189537
18.35	0.00208112	0.318	0.00208112
16.14	0.00227990	0.400	0.00227990
12.23	0.00260425	0.545	0.00260425
9.21	0.00283922	0.658	0.00283922
5.82	0.00309031	0.784	0.00309031
3.98	0.00322223	0.852	0.00322223
2.05	0.00335858	0.924	0.00335858

rect way. In the first variant (FEA 1), the aluminium beam was permanently connected with the concrete slab using the *tie* function to model full composite action (see Fig. 5a). In the second variant (FEA 2), surface-to-surface "hard" contact and friction (the coefficient of friction was 0.3) were defined between the flange of the aluminium beam and the edge of the concrete slab. Moreover, the aluminium beam and the concrete slab were connected using zero-length connectors (see Fig. 5b) to take slip into account. 12 points from the concrete slab were connected with the 12 points of the aluminium girder using zero-length wires. The type of connection was axial and the response of the connector was nonlinear. The orientation of the connector was specified using the coordinate system in which x direction was parallel to the length of the beam. The behaviour of

5. Results

The results of the analysis of the ACC beam with channel shear connectors are presented in Figs 6 and 7, and in Table 7.
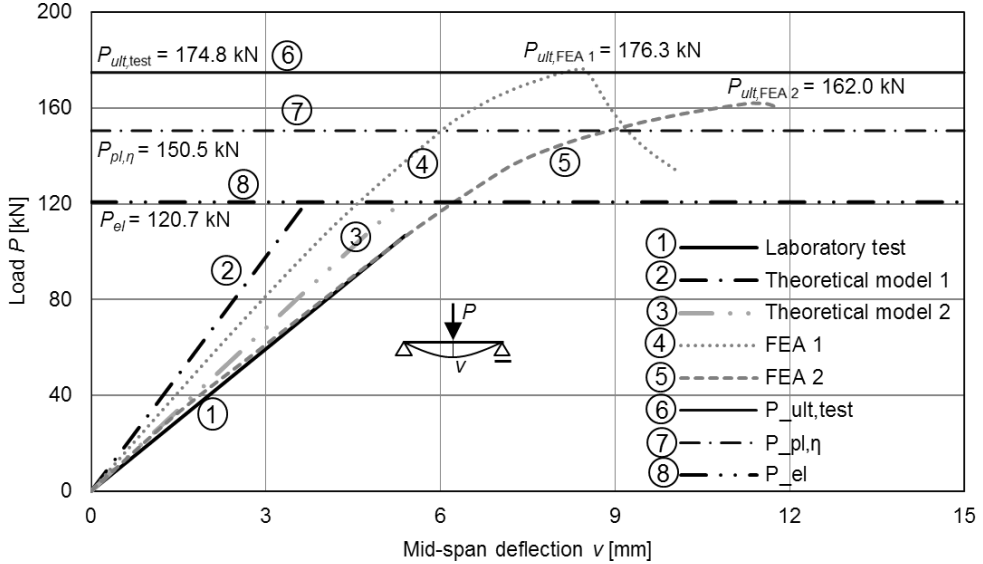

Fig. 6. Load-mid-span deflection curves from the theoretical and numerical analyses and the bending test [21] of the ACC beam.
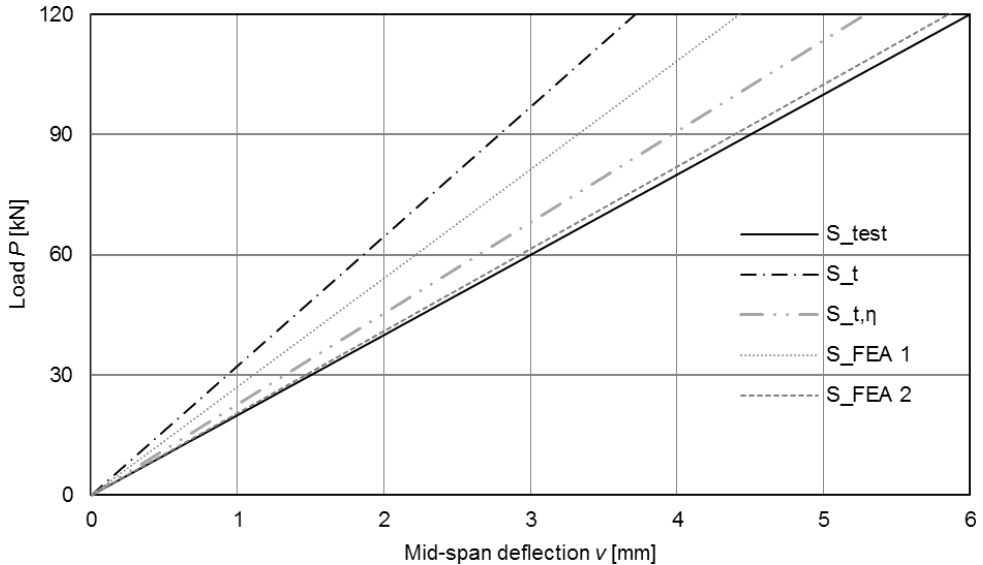

Fig. 7. Initial stiffness from the theoretical and numerical analyses and the bending test [21] of the ACC beam.

In the laboratory test presented in [21], the beam was tested using a three-point-bending test in the elastic and plastic ranges. Stonehewer demonstrated the results of the bending test in the elastic range (see curve 1 in Fig. 6) and the value of the load-bearing capacity of the tested beam ($P_{ult,\text{test}} = 174.8$ kN) (see curve 5 in Fig. 6) in his paper [21]. Curve 1 in Fig. 6 presents the elastic range of the bending test only, because Stonehewer did not present the plastic range in his paper.

Curve 2 presents the relationship between the load and the mid-span deflection curve in the theoretical model of the full composite beam. One can clearly see that curves 1 and 2 are different. What is more, the theoretical stiffness (32.3 kN/mm) was 1.6 times greater than the initial stiffness from the test (20.0 kN/mm). The difference was the result of the slip which occurred during the laboratory test. The slip had an impact on the stiffness of the ACC beam. Curve 3 presents the relationship between the load and the mid-span deflection curve in the theoretical model of the partial composite beam. The theoretical stiffness of the partial composite beam (22.7 kN/mm) was only 1.1 times greater than the initial stiffness from the bending test (20.0 kN/mm).

Curve 4 presents the relationship between the load and the mid-span deflection in the numerical model of bending of the ACC beam with full shear connection (FEA 1). Curve 5 presents the relationship between the load and the mid-span deflection curve in the numerical model of the ACC beam with partial interaction of the composite members (FEA 2). The bending plastic resistance of the ACC beam from FEA 1 (53.8 kN·m) was almost identical with the bending resistance from the test (53.3 kN·m) and 1.1 times higher than the bending plastic resistance of the ACC beam from FEA 2 (49.4 kN·m). The stiffness of the numerical model from FEA 1 (Curve 4) is higher than the stiffness of the numerical model from FEA 2 (Curve 5) and of the tested beam (Curve 1), because it was prepared for a full composite beam. Curves 1 and 5 overlap. The initial stiffness from FEA 2 (20.5 kN/mm) was almost identical with the initial stiffness from the test (20.0 kN/mm) (see Fig. 6). The numerical model with the zero-length connectors took slip into account and it adequately captured the elastic response of the ACC beam from the laboratory test conducted by Stonehewer.

In Table 9: Q_y – useful capacity of the connector calculated from Eq. (3.3), Q_{ult} – nominal shear strength of the channel shear connector calculated from Eq. (3.2), $Q_{y,\text{test}}$ – useful capacity of the connector from the test [21], $Q_{ult,\text{test}}$ – nominal shear strength of the channel shear connector from the test [21], P_{el} – load corresponding to the first yielding of the aluminium beam in the theoretical elastic model, P_{pl} – load corresponding to the bending plastic resistance of the ACC beam with full shear connection, $P_{pl,\eta}$ – load corresponding to the bending plastic resistance of the ACC beam with partial shear connection, $P_{ult,\text{test}}$ –

Table 9. The results of the theoretical and numerical analyses and the bending test [21] of the ACC beam.

Q_y [kN]	26.04	Q_{ult} [kN]	71.26	$Q_{y,\text{test}}$ [kN]	24.02
$Q_{ult,\text{test}}$ [kN]	77.84	P_{el} [kN]	120.7	P_{pl} [kN]	154.4
$P_{pl,\eta}$ [kN]	150.5	$P_{ult,\text{test}}$ [kN]	174.8	M_{el}[kN$\cdot$m]	36.8
M_{pl} [kN$\cdot$m]	47.1	$\text{M}_{pl,\eta}$ [kN$\cdot$m]	45.9	$M_{ult,\text{test}}$ [kN$\cdot$m]	53.3
$M_{el,\text{FEA 1}}$ [kN$\cdot$m]	47.2	$M_{el,\text{FEA 2}}$ [kN$\cdot$m]	43.3	$M_{ult,\text{FEA 1}}$ [kN$\cdot$m]	53.8
$M_{ult,\text{FEA 2}}$ [kN$\cdot$m]	49.4	S_t [kN/mm]	32.3	$S_{t,\eta}$ [kN/mm]	22.7
S_{test} [kN/mm]	20.0	$S_{\text{FEA 1}}$ [kN/mm]	27.1	$S_{\text{FEA 2}}$ [kN/mm]	20.5

load-bearing capacity of the ACC beam from the test [21], M_{el} – bending elastic resistance of the ACC beam from the theoretical model, M_{pl} – bending plastic resistance of the ACC with full shear connection from the theoretical model, $M_{pl,\eta}$ – bending plastic resistance of the ACC with partial shear connection from the theoretical model, $M_{ult,\text{test}}$ – bending resistance of the ACC beam from the test [21], $M_{el,\text{FEA 1}}$ – bending elastic resistance of the ACC beam from FEA 1, $M_{el,\text{FEA 2}}$ – bending elastic resistance of the ACC beam from FEA 2, $M_{pl,\text{FEA 1}}$ – bending plastic resistance of the ACC beam from FEA 1, $M_{pl,\text{FEA 2}}$ – bending plastic resistance of the ACC beam from FEA 2, $S_{\text{teoretical}}$ – initial stiffness of the ACC beam, $S_{\text{FEA 1}}$ – initial stiffness of the ACC beam from FEA 1, $S_{\text{FEA 2}}$ – initial stiffness of the ACC beam from FEA 2, S_{test} – initial stiffness of the ACC beam from the test presented in [21].

The capacity of the channel shear connector calculated from Eq. (3.2) (71.26 kN) was only 1.1 times lower than the one from the laboratory test (77.84 kN). It is possible to use Eq. (3.2) to estimate the capacity of the aluminium channel shear connector.

The bending plastic resistance of the ACC beam with partial shear connection from the theoretical model (45.9 kN$\cdot$m) was 1.2 times lower than the bending resistance from the test (53.3 kN$\cdot$m). The theoretical model which takes slip into account appears to be safe and makes it possible to calculate the bending plastic resistance of the ACC beam with partial shear connection.

6. Conclusions

The main conclusions of this paper are:

- The theoretical stiffness of the full composite beam (32.3 kN/mm) was 1.6 times greater than the initial stiffness from the laboratory test (20.0 kN/mm). The theoretical stiffness of the partial composite beam (22.7 kN/mm) was only 1.1 times greater than the initial stiffness from the test (20.0 kN/mm).

The impact of the slip on the stiffness of the ACC beam may be taken into account using the effective stiffness of the partial composite ACC beam calculated from Eq. (3.5).

- The capacity of the channel shear connector calculated from Eq. (3.2) was only 1.1 times lower than the one from the laboratory test. It seems that with the current state of knowledge, the proposed method of calculating the capacity of the channel shear connector is worth considering when designing ACC beams with channel shear connectors.

- The ACC beam analysed by Stonehewer in the laboratory test was a partial composite beam in which the slip occurred in the place of connection between both materials. The bending plastic resistance of the ACC beam with partial shear connection calculated from Eq. (3.4), which took slip into account, was 1.2 times lower than the bending resistance from the test (53.3 kN·m). The proposed method of calculating the bending plastic resistance of the ACC beam with partial shear connection is worth considering when designing ACC beams with channel shear connectors.

- The numerical model with the springs, the characteristics of which were taken from the push-out test, adequately captured the elastic response of the ACC beam from the laboratory test [21].

- The bending plastic resistance of the full composite aluminium-concrete beam from FEA 1 (53.8 kN·m) was 1.1 times higher than the bending plastic resistance of the partial composite aluminium-concrete beam from FEA 2 (49.4 kN·m). The slip reduced the bending resistance of the ACC beam.

- The stiffness of the numerical model from FEA 1 (Curve 3) is higher than the stiffness of the numerical model from FEA 2 (Curve 4) and of the tested beam (Curve 1), because the numerical model from FEA 1 was prepared for a full composite beam. The slip reduced the stiffness of the ACC beam.

- The initial stiffness from FEA 2 (20.5 kN/mm) was almost the same as the initial stiffness from the test (20.0 kN/mm). The numerical model with the zero-length wires took slip into account and it adequately captured the elastic response of the ACC beam from the laboratory test conducted by Stonehewer.

REFERENCES

1. Biegus A., Lorenc W., *Development of shear connections in steel-concrete composite structures*, Civil and Environmental Engineering Reports, **15**(4): 23–32, 2014, doi: 10.1515/ceer-2014-0032.

2. Lorenc W., Kożuch M., Rowiński S., *The behaviour of puzzle-shaped composite dowels – Part II: Theoretical investigation*, Journal of Constructional Steel Research, **101**: 500–518, 2014, doi: 10.1016/j.jcsr.2014.05.012.

3. Nie J., Cai C.S., *Steel-concrete composite beams considering shear slip effects*, Journal of Structural Engineering, **129**(4): 495–505, 2003, doi: 10.1061/(ASCE)0733-9445(2003)129:4(495).

4. Nie J., Cai C.S., Wang T., *Stiffness and capacity of steel-concrete composite beams with profiled sheeting*, Engineering Structures, **27**: 1074–1085, 2005, doi: 10.1016/j.engstruct.2005.02.016.

5. Leskelä M.V., *Shear connections in composite flexural members of steel and concrete*, ECCS, Technical Committee 11, Composite Structures, No 138, 2017.

6. Kuczma M., Kuczma B., *Composite steel-concrete beams with partial interaction: experimental, theory, simulation*, [in:] Katsikadelis J.T., Stavroulakis G.E. [Eds], *Recent advances in Mechanics. Book of abstracts, 9th German-Greek-Polish Symposium*, Orthodox Academy of Crete, Kolympari, Greece, September 4–9, Technical University of Crete, Chania, Greece, 2016, pp. 57–58 [e-book].

7. Szumigała M., Szumigała E., Polus Ł., *Laboratory Tests of New Connectors for Timber-Concrete Composite Structures*, Engineering Transactions, **66**(2): 161–173, 2018.

8. Polus Ł., Szumigała M., *Finite element modelling of the connection for timber-concrete composite beams*, IOP Conference Series: Materials Science and Engineering, **471**, article number: 052081, 2019, doi: 10.1088/1757-899X/471/5/052081.

9. Polus Ł., Szumigała M., *An experimental and numerical study of aluminium – concrete joints and composite beams*, Archives of Civil and Mechanical Engineering, **19**(2): 375–390, 2019, doi: 10.1016/j.acme.2018.11.007.

10. Feng R., Chen Y., Gong W., *Flexural behaviour of concrete-filled aluminium alloy thin-walled SHS and RHS tubes*, Engineering Structures, **137**: 33–49, 2017, doi: 10.1016/j.engstruct.2017.01.036.

11. Chen Y., Feng R., Xu J., *Flexural behaviour of CFRP strengthened concrete-filled aluminium alloy CHS tubes*, Construction and Building Materials, **142**: 295–319, 2017, doi: 10.1016/j.conbuildmat.2017.03.040.

12. Zhou F., Young B., *Concrete-filled aluminum circular hollow section column tests*, Thin-Walled Structures, **47**: 1272–1280, 2009, doi: 10.1016/j.tws.2009.03.014.

13. Bruzzese E., Cappelli M., Mazzolani F.M., *Experimental investigation on aluminium-concrete beams*, Construzioni Metalliche, **5**: 265–282, 1989.

14. Szumigała M., Polus Ł., *A numerical simulation of an aluminium-concrete beam*, Procedia Engineering, **172**: 1086–1092, 2017, doi: 10.1016/j.proeng.2017.02.167.

15. Siwowski T., *Aluminium bridges – past, present and future*, Structural Engineering International, **16**(4): 286–293, 2006, doi: 10.2749/101686606778995137.

16. MAZZOLANI F.M., *Structural applications of aluminium in civil engineering*, Structural Engineering International, **16**(4): 280–285, 2006, doi: 10.2749/101686606778995128.

17. SZUMIGAŁA M., POLUS Ł., *Applications of aluminium and concrete composite structures*, Procedia Engineering, **108**: 544–549, 2015, doi: 10.1016/j.proeng.2015.06.176.

18. HAG-ELSAFI O., ALAMPALLI S., *Cost-effective rehabilitation of two aluminum bridges on Long Island, New York*, Practice Periodical on Structural Design and Construction, **7**: 111–117, 2002, doi: 10.1061/(ASCE)1084-0680(2002)7:3(111).

19. MAZZOLANI F.M., *Aluminium structural design*, Springer-Verlag Wien, New York, 2003.

20. HÖGLUND T., TINDALL P., *Designers' guide to Eurocode 9: Design of aluminium structures, EN 1999-1-1 and -1-4*, ICE publishing, London, 2012.

21. STONEHEWER J., *A study of composite concrete-aluminum beams*, Master of Engineering, McGill University, Montreal, 1962.

22. KOSSAKOWSKI P., WCIŚLIK W., BAKALARZ M., *Selected aspects of application of aluminium alloys in building structures*, Structure and Environment, **9**(4): 256–263, 2017.

23. SKEJIĆ D., BOKO I., TORIĆ N., *Aluminium as a material for modern structures*, Gradevinar, **11**: 1075–1085, 2015, doi: 10.14256/JCE.1395.2015.

24. DAS S.K., KAUFMAN J.G., *Aluminium alloys for bridges and bridge decks*, [in:] Das S.K., Yin W. [Eds], *Aluminium alloys for transport, packing, aerospace and other applications*, Warrendale (USA): The Minerals, Metals & Materials Society, 2007.

25. PHAM N.H., PHAM C.H., RASMUSSEN K.J.R., *Incorporation of measured geometric imperfections into finite element models for cold-rolled aluminium sections*, [in:] Tran-Nguyen H. *et al.* [Eds], Proceedings of the 4th Congrès International de Géotechnique – Ouvrages – Structures, Springer Nature Singapore Pte Ltd., 2018, pp. 161–171.

26. ALISON G.A., *Evaluation of seven aluminum highway bridges after two to three decades of service*, Transportation Research Record, **950**: 123–129, 1984.

27. DOKŠANOVIĆ T., DŽEBA I., MARKULAK D., *Applications of aluminium alloys in civil engineering*, Technical Gazette, **24**(5): 1609–1618, 2017, doi: 10.17559/TV-20151213105944.

28. SZUMIGAŁA M., CHYBIŃSKI M., POLUS Ł., *Preliminary analysis of the aluminium-timber composite beams*, Civil and Environmental Engineering Reports, **27**(4): 131–141, 2017, doi: 10.1515/ceer-2017-0056.

29. CHYBIŃSKI M., POLUS Ł., RATAJCZAK M., SIELICKI P.W., *The evaluation of the fracture surface in the AW-6060 T6 aluminium alloy under a wide range of loads*, Metals, **9**(3), 2019, article number: 9030324, doi: 10.3390/met9030324.

30. ROM S., AGERSKOV H., *Fatigue in aluminum highway bridges under random loading*, International Journal of Applied Science and Technology, **4**(6): 95–107, 2014.

31. MARCINOWSKI J., *Stresses in a layered, composite structure fabricated from materials of different thermal expansions* [in Polish], Materiały Budowlane, **4**: 107–109, 2018.

32. GWÓŹDŹ M., *Project problems of contemporary aluminium structures* [in Polish], Czasopismo Techniczne, **104**(z. 4-A): 281–286, 2007.

33. OKURA I., *Application of aluminium alloys to bridges and joining technologies*, Welding International, **17**(10): 781–785, 2003, doi: 10.1533/weli.17.10.781.22037.

34. SKEJIĆ D., ĆURKOVIĆ I., JELČIĆ RUKAVINA M., *Behaviour of aluminium structures in fire, A review*, [in:] Wald F., Burgess I., Jelčic Rukavina M., Bjegovic D., Horova K. [Eds], Proceedings of 4th International Conference Applications of Structural Fire Engineering in Dubrovnik, Croatia, 15–16 October, 2015, doi: 10.14311/asfe.2015.047.

35. POLUS Ł., CHYBIŃSKI M., SZUMIGAŁA M., *Bending resistance of metal-concrete composite beams under standard fire conditions* [in Polish], Przegląd Budowlany, **7-8**: 128–132, 2018.

36. CHYBIŃSKI M., POLUS Ł., *Bending resistance of metal-concrete composite beams in a natural fire*, Civil and Environmental Engineering Reports, **4**(28): 149–162, 2018, doi: 10.2478/ceer-2018-0058.

37. SIWOWSKI T., *Aluminium road bridges – past, present and future* [in Polish], Roads and Bridges, **1**: 39–74, 2005.

38. POLUS Ł., SZUMIGAŁA M., *Tests of shear connectors used in aluminium-concrete composite structures*, [in:] Giżejowski M., Kozłowski A., Marcinowski J., Ziółko J. [Eds], *Recent Progress in Steel and Composite Structures*, CRC Press-Taylor & Francis Group, Boca Raton, 2016, pp. 133–136.

39. European Committee for Standardization, EN 1994-1-1, *Eurocode 4, Design of composite steel and concrete structures – Part 1-1: General rules and rules for buildings*, Brussels, 2004.

40. JOHNSON R.P., *Designers' guide to Eurocode 4: Design of composite steel and concrete structures, EN 1994-1-1*, ICE Publishing, London, 2012.

41. DUMOVIĆ D., ANDROIĆ B., LUKAČEVIĆ I., *Composite structures according to Eurocode 4, Worked Examples*, Ernst & Sohn, Berlin, 2015.

42. KURZAWA Z., RZESZUT K., SZUMIGAŁA M., *Steel rod structures, Part III: Structures with arches, thin-walled elements, membrane coverings, composite elements, ring roofs and gantry beams* [in Polish: *Stalowe konstrukcje prętowe, Część III: Konstrukcje z łukami, elementy cienkościenne, pokrycia membranowe, elementy zespolone, dachy pierścieniowe i belki podsuwnicowe*], Wydawnictwo Politechniki Poznańskiej, Poznań, 2017.

43. ANSI/AISC 360-16, *Specification for structural steel buildings*, American Institute of Steel Construction, Chicago, 2016.

44. ŁUKASZEWSKA E., *Development of prefabricated timber-concrete composite floors*, PhD Thesis, Lulea University of Technology, 2009.

45. ŁUKASZEWSKA E., JOHNSSON H., FRAGIACOMO M., *Performance of connections for prefabricated timber – concrete composite floors*, Materials and Structures, **41**: 1533–1550, 2008, doi: 10.1617/s11527-007-9346-6.

46. HASSANIEH A., VALIPOUR H. R., BRADFORD M.A., *Experimental and analytical behaviour of steel-timber composite connections*, Construction and Building Materials, **118**: 63–75, 2016, doi: 10.1016/j.conbuildmat.2016.05.052.

47. European Committee for Standardization, EN 1995-1-1, Eurocode 5, *Design of timber structures – Part 1–1: Common rules and rules for buildings*, Brussels 2004.

48. *Abaqus 6.13 Documentation*, Abaqus Analysis Users Guide, Abaqus Theory Guide.

49. JANKOWIAK T., ŁODYGOWSKI T., *Quasi-Static Failure Criteria for Concrete*, Archives of Civil Engineering, **LVI**(2): 123–154, 2010, doi: 10.2478/v.10169-010-0007-8.

50. JANKOWIAK I., *Case study of flexure and shear strengthening of RC beams by CFRP using FEA*, AIP Conference Proceedings, **1922**(1): 130004, 2018, doi: 10.1063/1.5019134.

51. SZEWCZYK P., SZUMIGAŁA M., *Static equilibrium paths of steel-concrete composite beam strengthened under load*, Civil and Environmental Engineering Reports, **28**(2): 101–111, 2018, doi: 10.2478/ceer-2018-0022.

52. European Committee for Standardization, EN 1992-1-1, *Eurocode 2, Design of concrete structures – Part 1–1: General rules and rules for buildings*, Brussels, 2004.

53. KMIECIK P., KAMIŃSKI M., *Modelling of reinforced concrete structures and composite structures with concrete strength degradation taken into consideration*, Archives of Civil and Mechanical Engineering, **11**(3): 623–636, 2011, doi: 10.1016/S1644-9665(12)60105-8.

54. BAZANT Z.P., BECQ-GIRAUDON E., *Statistical prediction of fracture parameters of concrete and implications for choice of testing standard*, Cement and Concrete Research, **32**: 529–556, 2002, doi: 10.1016/S0008-8846(01)00723-2.

55. Comite Euro-International du Beton, *CEB-FIP Model Code 1990*, Thomas Telford, London, 1991.

56. HORDIJK D.A., *Local approach to fatigue of concrete*, PhD Thesis, Delft University of Technology, 1991.

57. POLUS Ł., SZUMIGAŁA M., *Laboratory tests vs. FE analysis of concrete cylinders subjected to compression*, AIP Conference Proceedings, **2078**, article number: 020089, 2019, doi: 10.1063/1.5092092.